Natural Hazards
https://doi.org/10.1007/s11069-020-03917-w

ORIGINAL PAPER

Anthropogenically induced subsidence in Thessaly, central Greece: new evidence from GNSS data

Panagiotis Argyrakis[1,2] · Athanassios Ganas[2] · Sotirios Valkaniotis[3] · Vasilios Tsioumas[4] · Nikolaos Sagias[1] · Basil Psiloglou[5]

Received: 26 April 2019 / Accepted: 31 March 2020

Abstract
We combine almost 10 years of continuous GNSS observations at four permanent stations with groundwater and rainfall data to investigate subsidence patterns in the region of Thessaly, central Greece. Thessaly is a key area for studying anthropogenic versus tectonic subsidence in Greece because it is (a) characterized by overexploitation of groundwater reservoirs since the 1980s and (b) has a Twentieth-century history of shallow, normal-slip earthquakes with $M > 6$. We infer that anthropogenic subsidence continues at southeast Thessaly (Karla reservoir region) up to autumn of 2017 because the vertical time-series data of station STEF (Stefanovikio) reach a cumulative value of 55 cm and show a "ramp-flat" pattern that correlates with neighboring borehole data. The geodetic data from other three examined regions (city of Larissa, city of Karditsa and Klokotos) indicate ground stability. The GNSS stations in Karditsa (KRDI) and Larissa (LARM) show correlation with groundwater-level fluctuations but no subsidence. Station KLOK (Klokotos) shows a small subsiding trend (−0.38 mm/yr) with no correlation to either groundwater levels or to rainfall patterns; therefore, its seasonal periodicity may reflect geodynamic (plate) motions.

Keywords Thessaly · Subsidence · GNSS · Time-series · Groundwater · Hazard

1 Introduction

The region of Thessaly, in Central Greece (Fig. 1), is well known for its land subsidence phenomena since the 1980s (Zouros et al. 1994; Soulios 1997; Rapti-Caputo and Caputo 2004; Kontogianni et al. 2007; Apostolidis and Koukis 2013; Ilia et al. 2018). During the last five decades, this region of Greece exhibits an intensive development, mainly based on mechanized agriculture and changes in crop patterns. Because of the large need for irrigation several thousand boreholes have been drilled. However, the overexploitation of the ground water has triggered the manifestation of land subsidence phenomena. These

Electronic supplementary material The online version of this article (https://doi.org/10.1007/s11069-020-03917-w) contains supplementary material, which is available to authorized users.

✉ Panagiotis Argyrakis
pargyrak@noa.gr

Extended author information available on the last page of the article

Published online: 10 April 2020

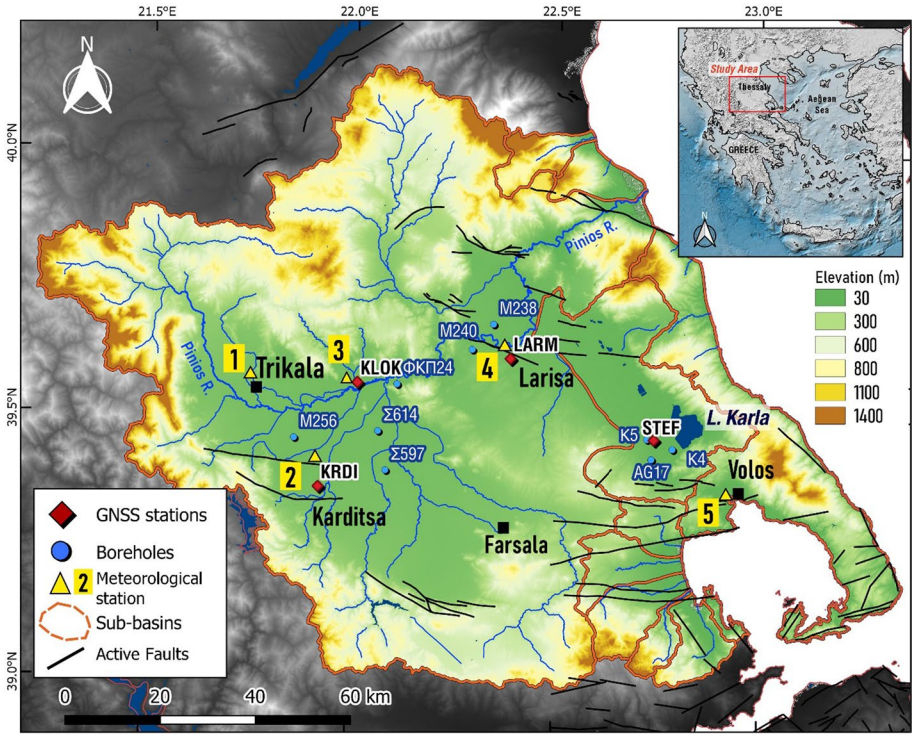

Fig. 1 Elevation map of Thessaly (see inset box for its location within Greece) showing locations of GNSS stations (red rhombs), boreholes (cyan circles) and active faults (black lines; Ganas et al. 2013a, b). Black squares represent important towns mentioned in text. Drainage is shown in blue. The orange polygons indicate the boundaries of the hydrological basin (and sub-basins) of Thessaly. Yellow triangles indicate the sites of meteorological stations used in this study, 1: Trikala, 2: Karditsa, 3: Klokotos, 4: Larisa, 5: Volos

phenomena have been studied during the last 20 years by many researchers, who have supplied an extensive set of geological, geotechnical and geodetic data (especially InSAR techniques; Salvi et al. 2004; Atzori et al. 2005; Ganas et al. 2006; Parcharidis et al. 2011; Vassilopoulou et al. 2013; Modis and Sideri 2015; Ilia et al. 2016, 2018; Foumelis et al. 2016). Land subsidence in the Thessaly Plain in central Greece was first documented using ERS (C-band) images acquired between 1992 and 2002 (e.g., Salvi et al. 2004; Ganas et al. 2006; Ilia et al. 2016). The consensus from previous studies was that subsidence is driven by local anthropogenic activity, such as (a) due to the compaction of unconsolidated sediments that results from exploitation of groundwater and (b) due to urbanization. It is therefore important to monitor the ongoing subsidence and its spatiotemporal characteristics because it allows the development of mitigation strategies that could minimize the risk of damage to both surface structures and infrastructures.

Until the mid-Twentieth century the Thessaly plains were covered by swamps, small lakes and river floodplains. Following the construction of extensive water discharge channels, Lake Karla in SE Thessaly (Fig. 1) was drained at 1962, and this area (~180 km^2) was progressively given to agriculture (in the 1960s). Since the 1980s the rapid economic development led to an increasing need for water, provided by productive boreholes. Furthermore, overexploitation of the aquifers of the Pinios basin (see Fig. 1) was enhanced

by water over-pumping conducted by the water supply organizations of the urban centers of Thessaly to meet the increasing needs, since these were the main providers of drinking water. The effects of subsidence in eastern Thessaly were first noticed in the late 1980s in the form of large ground cracks affecting crops and built areas. Since then, the morphological and environmental setting of the region has changed, leading to a government decision to restore the former Karla lake by building an artificial reservoir toward the restoration of water balance and the reversal of environmental degradation (Loukas et al. 2007; Sidiropoulos et al. 2013). In particular, comparison of maps and aerial photographs covering a period of up to 40 years and of more recent geodetic data revealed that in this area a cumulative subsidence of several meters had occurred between 1970 and 2010 (Soulios 1997; Kontogianni et al. 2007). Subsidence has been correlated with strata lithology, formation, and structure (Kontogianni et al. 2007; Ilia et al. 2018). For example, dewatering of loose soil layers in which the water provides structural support produces surface subsidence with the following sequence of processes: Groundwater is extracted from a shallow aquifer; groundwater levels decline which reduces structural support, causing volumetric contraction of (primarily) fine-grained sediment resulting in land subsidence. Consequently, the depth of groundwater exploitation and its variations with time control the magnitude of land subsidence (e.g., Rapti-Caputo and Caputo 2004; Stamatopoulos et al. 2018). Agricultural activity that relies significantly on irrigation (e.g., cotton) contributes to the groundwater depletion in aquifer systems of fine-grained sediments. Water-level monitoring using piezometers (e.g., Rapti-Caputo and Caputo 2004; Ilia et al. 2018; Seferli et al. 2019) and InSAR (e.g., Foumelis et al. 2016 and references therein ; Ganas et al. 2004) have been used to understand the spatiotemporal variations of groundwater depletion. Exploitation of aquifers decreases the groundwater volume, causing land subsidence that can be detected by GNSS (e.g., Zerbini et al. 2007; Ustun et al. 2010; Ganas et al. 2016; Serpelloni et al. 2018).

The purpose of this study is to point out the use of long time series of geodetic data in monitoring ground motions in relation to both precipitation and groundwater data. We show that the 2008–2018 geodetic data indicate the continuing manifestation of the land subsidence in the SE Thessaly, while in the rest of the region ground motions are negligible. We also highlight the anthropogenic phenomena as a geohazard that causes slow ground deformations and as a threat for both the natural and urban environment.

2 Geology and tectonics

The geology of Thessaly consists of basement (pre-rift; mostly carbonate rocks and schists) and sedimentary (syn-rift) rocks. The latter mainly comprise marls of Pliocene age and terrestrial sands and gravels of Pleistocene age, with silt to silty clay intercalations. The multiple alternations of permeable coarse-grained deposits (aquifers) with impermeable to low-permeability strata (aquitards) create a number of successive semi-confined to confined aquifers. There are highly compressible units, which may be responsible for subsidence phenomena in both urban and agricultural areas.

In terms of tectonic setting Thessaly is located at the western end of the North Anatolian Fault Zone (NAFZ) in north Aegean Sea, where the right-lateral slip along this plate-boundary structure ends and crustal extension prevails in mainland Greece (Hatzfeld et al. 1999; Kahle et al. 2000). The most prominent structural and geomorphic features strike NW–SE, such as the coastal and interior mountain ranges, their bounding faults and the

late Tertiary sedimentary basins (Caputo and Pavlides 1993). However, the Early Quaternary-to-present tectonic regime has formed WNW–ESE and E–W high angle, normal and oblique faults (Fig. 1; Mountrakis et al. 1993; Caputo and Pavlides 1993; Caputo et al. 1994; Pavlides et al. 2004). The recent activity of these structures is confirmed by the location and focal mechanisms of small- and large-magnitude earthquakes around Thessaly (Papazachos et al. 1983; Papastamatiou and Mouyaris 1986; Pavlides 1993; Hatzfeld et al. 1999; Pavlides et al. 2004; Ganas et al. 2014) and by paleoseismological data (e.g., Caputo et al. 2004; Palyvos et al. 2010; Tsodoulos et al. 2016). The most seismically active part is south Thessaly where four, large earthquakes occurred, in 1954 ($M=7.0$; Palyvos et al. 2010), in 1955 ($M=6.2$; Ambraseys and Jackson 1990), in 1957 ($M=6.8$; Papazachos et al. 2016) and in 1980 ($M=6.5$; Papazachos et al. 1983; Drakos et al. 2001). An $M=6.1$ shallow event occurred near Larisa in 1941 causing extensive damage to villages along the east margin of the plain (Ambraseys and Jackson 1990). There is a notable increase in crustal strain intensity from North toward South, inside Thessaly (Chousianitis et al. 2013a, 2015), which correlates well with the increased seismicity rates in that area.

3 The use of GPS to study surface movements in Greece

The GPS/GNSS geodetic technique has been applied to investigate Earth surface movements and to map tectonic strain patterns in Greece and surrounding regions (e.g., Clarke et al. 1998; McClusky et al. 2000; Serpelloni et al. 2005; Ganas et al. 2008, 2013b, 2018a, b; Chousianitis et al. 2013a, 2015; Marinou et al. 2015; Devoti et al. 2017). The Thessaly area contains important active faults located on-shore; they are capable of rupturing with events with $6<M<7$ (e.g., Caputo 1990; Caputo and Pavlides 1993; Drakos et al. 2001; Mountrakis et al. 1993; Papazachos et al. 1993; Pavlides et al. 2004; Palyvos et al. 2010; see Fig. 1), so tectonic deformation is expected, and therefore, GNSS is suited as observation technique. The advantage of GNSS is the comparable accuracy (mm level in post-processing mode) that offers in comparison with costly geometric and trigonometric leveling campaigns, while the GNSS data are immediately available via the Internet as most institutions have adopted the open-data policy promoted by EU.

Historical GPS data (Clarke et al. 1998; McClusky et al. 2000; Nyst and Thatcher 2004) indicate that Thessaly is undergoing extension in the general N-S direction with considerable variations (up to 45°) due to the sparse coverage of campaign stations. According to the data of McClusky et al. (2000) the overall region is rapidly extending at a rate of about 10 mm/yr. Denser data from the Central Greece GPS Network (Clarke et al. 1998) show in central Thessaly small-scale variations of the velocity field. Nyst and Thatcher (2004) include central and south Thessaly in their "central Greece" block, with a general NW–SE extension direction and its northern boundary to cross Thessaly from ESE to WNW. Using continuous GPS data Chousianitis et al. (2013a, 2015) showed that tectonic strain in Thessaly is small (nearly 10–20% of what is accumulated across the major rift systems of Greece further south (i.e., Corinth rift)), while the extensional strain axis is oriented N-S. Most of these studies examine the strain originating from the two horizontal components of the velocity field, as it was expected that horizontal motions were the most important.

In our study, the geodetic measurements from permanent GNSS stations integrated with other geological and geophysical information, will be used to constrain patterns of surface subsidence. Our first objective is to establish both the magnitude and direction of the vertical component of the velocity. The geodetic data will be also compared to groundwater

table measurements from 9 boreholes (Fig. 1), provided by the Institute of Geological and Mineral Exploration (IGME), Athens. We also collected rainfall data from several meteorological stations in Thessaly in order to investigate any possible seasonal loading effects (e.g., Argus et al. 2014).

4 GPS data and methods

4.1 Permanent stations and data quality

We processed GPS data (30-s sampling interval) from the following permanent networks: NOA (Ganas et al. 2008, 2013b) and METRICA (commercial provider in Greece; http://www.metricanet.gr/). The location of the stations is shown in Fig. 1, and field photographs of geodetic antennas are included in Fig. 2. Station KLOK and STEF belong to the national geodetic network of the Institute of Geodynamics—National Observatory of Athens

Fig. 2 Field photographs showing geodetic antennas used in this study: Station KLOK (top left), Station LARM (top right), Station KRDI (bottom left), Station STEF (bottom right)

(NOANET; http://www.gein.noa.gr/services/GPS/noa_gps.html). Station KRDI belongs to METRICANET, and station LARM is part of the Aristotle University of Thessaloniki and EPN-EUREF networks. All stations are equipped with dual-frequency geodetic (GNSS) receivers, while two stations (KLOK and LARM) are equipped with choke-ring antennas (see Table 1 for details; Fig. 2). Data coverage per station varies from 5 to 10 years of observations (Table 1).

After collecting all the necessary GPS data in RINEX format a preprocessing procedure was applied to assure that the collected data have the best quality to proceed in estimating daily station static positions. First, we used the TEQC software (Estey and Meertens 1999) to extract multipath and other quality quantities. The generation of multipath effect is being taking place when a signal received to antenna from multiple paths than from direct one. Clearly it depends from the satellite geometry and mainly from the surrounding environment. The received signal from other paths than from direct induces a delay to the arrival because it gets longer to be received from the antenna and also introduces an error to carrier phase and pseudorange measurements (Kaplan and Hegarty 2006). Sometimes we observe negative values that occur when direct and reflected signal interfere and they are out of phase. A multipath analysis for 30-s daily data from the four, dual-frequency stations in Thessaly (KLOK, KRDI, LARM and STEF) is presented in supplementary Figure S1. All multipath levels are minimal and stable through time, at both GPS frequencies.

4.2 Processing of GPS data

The GPS data were processed with the GIPSY/OASIS II software (ver. 6.4) developed by Jet Propulsion Laboratory (JPL; http://gipsy-oasis.jpl.nasa.gov; Bertiger et al. 2010). This software is using a Precise Point Positioning strategy (PPP; Zumberge et al. 1997). The main advantage of the PPP method is that it allows to easy diagnose receiver-specific problems, with root-mean-square (rms) value of postfit residuals; if those are excessively noisy it may be indication of hardware failure, interfering radiofrequencies (RF), excessive multipath environment or other unusual phenomena. Another advantage of this method is that is saves computational time since instead of analyzing tens of stations we need only the specific station to produce results.

The geodetic data were 30 s RINEX v2.11 files from the four stations (KLOK, LARM, STEF, KRDI). We used the orbit and clock files of highest precision (*flinnR* files from JPL). We used zenith tropospheric estimation according to international guidelines and experience (e.g., Hill and Blewitt 2006; a value of 5×10^{-8} cm/s^2 random walk noise is recommended); we used the tide model *WahrK1* (Wahr 1985) and we added an ocean load tide model (*OcnldCpn*) which uses 11 tidal frequencies to infer other frequencies; we added troposphere gradients, and our experience has shown that a recommended random walk value for static positioning is 5×10^{-9} cm/s^2; we adopted the troposphere mapping function GPT2 (Global Pressure and Temperature Mapping Function; Rózsa 2014) which was shown to be better than the NIELL mapping function (Wang and Li 2016) and provides similar results as the VMF1 model (Vienna Mapping Function). We find the use of GPT2 more appropriate because we analyze long-term recording GNSS stations (Steigenberger et al. 2009; so we keep the advantage not to maintain a tropospheric database for this purpose); we calculated and generated receiver antenna calibration file for each station separately from IGS ATX file (from http://www.igs.org/wg), and finally we defined a lower elevation angle cutoff of 10° to minimize near-field multipath effect. The produced position time series were analyzed by *TSAnalyzer* (Wu et al. 2017) with the use of least square

Table 1 Characteristics of GNSS stations in Thessaly. Station coordinates are in decimal degrees, height is in m

Name	Location	LAT	LON	Height (ellips.)	Antenna	Receiver	Data start	Data end
KLOK	Klokotos	39.564	22.014	135.8	AT504 LEIS	LEICA GRX1200PRO	2008-07-17	2018-08-18
KRDI	Karditsa	39.366	21.922	157.6	LEIAR10	LEICA GR10	2012-06-08	2018-08-11
STEF	Stefanovikio	39.464	22.742	98.0	ASH111661	ASHTECH PF500	2012-09-14	2017-07-21
LARM	Larissa	39.614	22.387	151.3	LEIAR25	LEICA GRX1200+GNSS	2011-01-20	2018-06-30

estimation (see Supplementary Figure S2); we obtained the residuals (see Supplementary Figure S3), and by the usage of interquartile range (IQR) which is a measure of statistical dispersion, being equal to the difference between 75th and 25th percentiles (Upton and Cook 1996), we removed any outlier so as to get "cleaner" data; then we applied least square analysis to obtain the linear trend (see Table 2) and any harmonic components. The noise removal was done by use of CATS software (Williams 2008). The vertical, de-noised component of the position time series is shown in Fig. 3.

4.3 Geodetic results

We estimated station velocities (north, east, up components) and their 1-σ uncertainties (Table 2). We show the station position time series (all components) as Supplementary figure S2 and the residuals of the time series as Supplementary figure S3. Our 10-yr solution results for station KLOK compare well with the 5-yr solution result by Chousianitis et al. (2013b) obtained by the GAMIT software. The difference between our results and previously published solutions is within 0.26 mm/yr on the horizontal components (E, N) and 0.68 mm/yr. on the vertical (Up). Both GIPSY and GAMIT up solutions indicate a downward trend; however, the GIPSY result is considered more stable (-0.38 mm/yr ± 0.02; Table 2) because of the longer data span (10 years of data are presented in this paper).

At the vertical component of KLOK, LARM and KRDI we observe a periodical seasonal signal (period less than one year) which is rigorously analyzed in discussion section. The vertical component at KLOK, LARM and KRDI fluctuates with respect to a mean value (near 0) plus or minus a few cm (± 2 cm for KLOK; ± 1.5 cm for KRDI; and ± 2 cm for LARM) (Fig. 3). The position residuals of these stations do not exceed 1 cm on the vertical (Supplementary Fig. S3; except for STEF). Station STEF displays a different behavior: The vertical component shows a continuous decrease in position (indicating subsidence) reaching 55 cm during 5 years (2012–2017; lower panel in Fig. 3). The curve of the vertical shows a "flat-ramp" behavior, that is "flat" positions are maintained during winter, spring, autumn and a "ramp" during summer. The vertical position does not recover as in the cases of the other three stations, but it shows a downward trend. The rapid subsidence of STEF indicates that this station should not be used in tectonic strain studies.

5 Discussion

5.1 Geodetic data relation to groundwater levels

The GNSS analysis shows the presence of a subsidence mainly localized in the vicinity of station STEF in Thessaly's southeast area. In the large Larissa plain, due to continuing strong farming practices, a rapid subsidence is observable over the Stefanovikio–Karla area (Fig. 4). In all remaining areas (north Thessaly, west Thessaly) the periodic component of the GNSS vertical signal probably reflects other processes such as global plate motions, orogenic uplift processes (Chen et al. 2018), groundwater motions inside karst systems (e.g., Serpelloni et al. 2018) or shallow water table fluctuations connected with pumping for field irrigation. We elaborate on this more by presenting groundwater data and correlation analysis below. Possible additional causes of the ground subsidence in alluvial plains are: (1) the consolidation of near-surface sediments; (2) the oxidation of peat soils in the vadose zone; (3) the subsurface instability of mud layers caused by the consolidation of

Table 2 GNSS station velocities (north, east, up) estimated in the ITRF2008 reference frame together with their 1-σ uncertainties

Name	Epochs	N-linear (mm/yr)	E-linear (mm/yr)	Up-linear (mm/yr)	S-north (mm/yr)	S-east (mm/yr)	S-up (mm/yr)
KLOK	3169	5.913	21.000	− 0.385	0.007	0.007	0.027
KRDI	1906	6.299	19.473	− 0.502	0.016	0.015	0.059
LARM	2205	4.623	21.310	− 0.036	0.012	0.012	0.047
STEF	1369	− 1.365	11.063	− 119.075	0.030	0.045	0.292

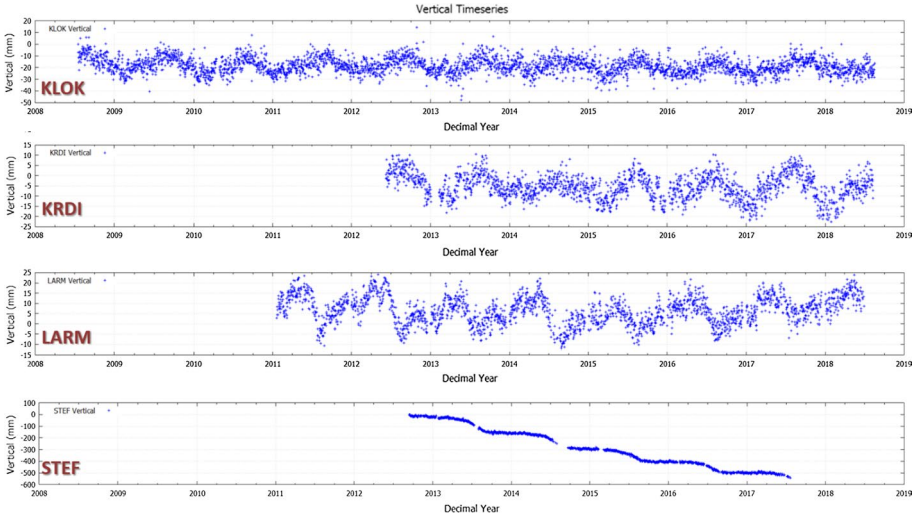

Fig. 3 Time-series plots of daily vertical position estimates of stations KLOK, KRDI, LARM and STEF (see Fig. 1 for location) referred to the ITRF2008 reference frame. *X*-axis is time (years), *Y*-axis is position (in mm). Notice the large (0.55 m) cumulative subsidence of station STEF

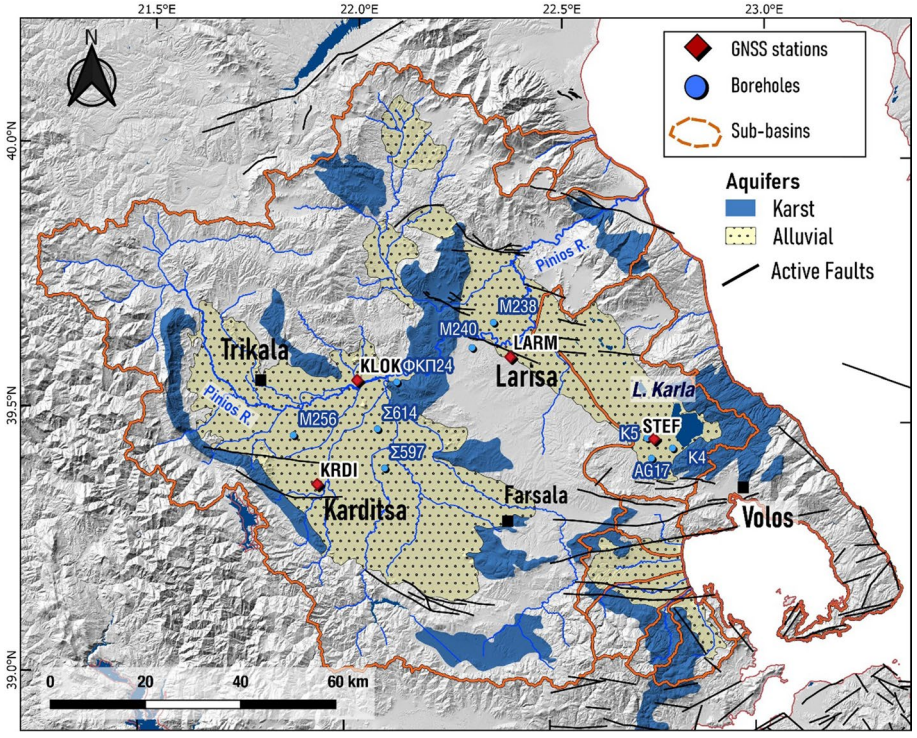

Fig. 4 Relief map of Thessaly showing locations of groundwater boreholes near the GNSS stations. Background colors indicate the nature of groundwater storage (karstic vs alluvial). Black lines are active faults

relatively deep layers; (4) anthropogenic effects, such as compaction of surface sedimentary strata, caused by groundwater pumping (e.g., (Rapti-Caputo and Caputo 2004; Kontogianni et al. 2007).

Thessaly plain is formed by two separate large alluvial aquifers (Fig. 4): the western Thessaly plain aquifer that extends along Trikala and Karditsa plain, and the eastern Thessaly plain aquifer that covers the area of Larissa and Karla plains. These two large aquifer systems have multiple confined aquifers developed in a thick sequence of Pliocene to Holocene sediments that reach a thickness of up to 450 m. At the borders of the two alluvial plains, a series of smaller karst aquifers are present in thick carbonate formations (e.g., Manakos et al. 2019) that contribute to groundwater inflow into the alluvial aquifers of the plains. Although both large alluvial aquifer systems are part of the Pinios hydrological basin (Fig. 1), groundwater connection is limited, if present at all (Manakos and Tsioumas 2010). GNSS stations LARM and STEF are positioned in the eastern Thessaly alluvial aquifer (Fig. 4). KRDI station is positioned inside the western Thessaly alluvial aquifer. KLOK station, while being inside the same alluvial plain, is founded on marble bedrock that is part of the karst aquifer systems at the northeast border of western Thessaly alluvial plain. Although the exact groundwater conditions are not known in detail, the local karst aquifer below KLOK station is believed to be connected with the surrounding thick alluvial aquifer (Manakos and Tsioumas 2010).

The variation of the mean piezometric level has been studied using several deep water boreholes across the basin (Fig. 4) with available data for the period 2008–2018. The ground water network has been measured regularly by the Institute for Geological and Mineral Exploration (IGME). We selected two or three boreholes in the vicinity of each GNSS station (Fig. 5), so we can explore the variability in groundwater levels in relation to the time series of the vertical component of the position. The distances between boreholes and GNSS stations are reported in Supplementary Table S1. Boreholes AG17, K4 and K5 are located close to station STEF (Fig. 5) where the largest subsidence was measured. The groundwater data are presented in Fig. 6. In all three boreholes the groundwater level range was from −40 m to −75 m (Fig. 6), indicating a rather homogeneous behavior of the aquifer, although K4 and K5 levels are shallower than AG17. The data indicate that during the last decade, an especially close to regions where the surface elevation was reduced (such as station STEF), the drawdown reaches 20 m (see the year 2014 in borehole AG17; Fig. 6a). In two other boreholes, K4 and K5, located within 4 km from STEF, we observed fluctuations reaching 25 m (maximum; see K4 data in Fig. 7) in range, since 2008. Furthermore, in K4 we observe a 15-m drop during year 2014 following the 25-m drop during 2013 and followed by a 6-m drop in 2015 (see Fig. 7). In those years the lows are recorded either in the summer of 2013 (−67 m) or in the autumn of 2014 (−58 m) or in the autumn of 2015 (−53 m). The data of K5 also confirm that year 2013 was marked by a general fall of groundwater levels in the vicinity of STEF as the drawdown reached 24 m (Fig. 7). The data indicate that in the greater area of village Stefanovikio (Fig. 5) there is considerable drop in groundwater level which can be associated with observed surface subsidence in geodetic data (Fig. 7). Our vertical time-series results for station STEF (Fig. 7) indicate the following: During the summer of 2013, the drawdown was 16 cm, during the summer of 2014 the drawdown was 15 cm, during the summer of 2015, the drawdown was 10 cm, and during the summer of 2016, the drawdown was 10 cm, respectively. On the contrary, station LARM (Fig. 3; see panel LARM) was not severely affected by groundwater-level variations which were observed in boreholes M238 during the summer of 2014 (12-m drawdown; Fig. 6a panel M238) and during

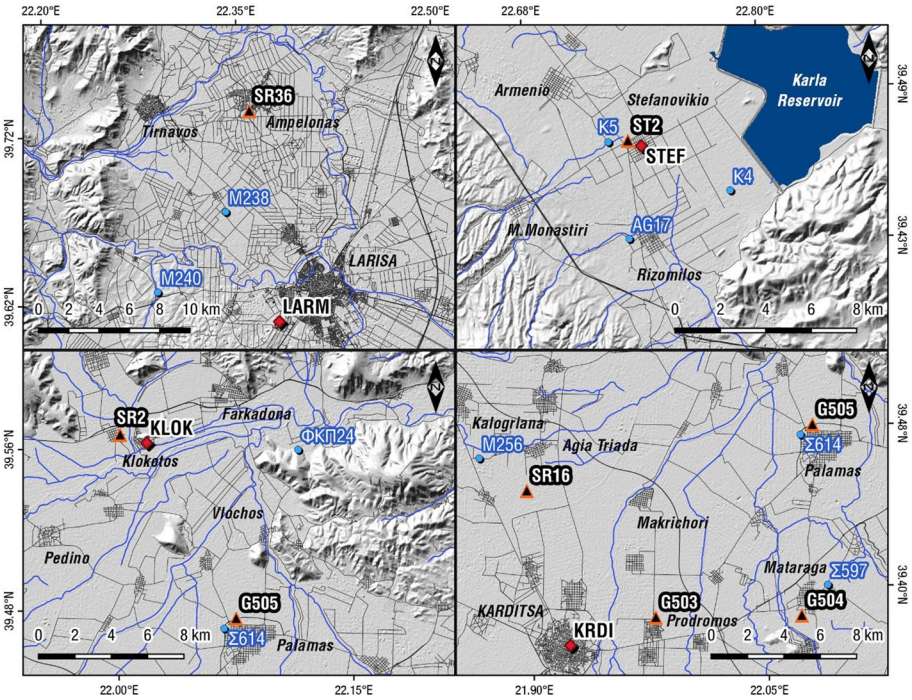

Fig. 5 Relief maps of Thessaly showing topography, urban fabric, boreholes, river and road networks near the four GNSS stations (red rhombs), LARM (top left), STEF (top right), KRDI (bottom right) and KLOK (bottom left). The groundwater-level variations from selected boreholes are shown in Figs. 6 and 7 (period 2008–2018). Black/orange triangles show the location of boreholes with available lithological data

the summer of 2015 (9-m drawdown; Fig. 6a) and M240 during the summer of 2013 (8-m drawdown; Fig. 6b). We do observe a systematic low in the time series of LARM at the end of the summer of 2013, 2014, 2015, and 2016 but the elevations recover during the subsequent winters. Station KRDI is subjected to the groundwater-level fluctuations, as well (see S597 data in Fig. 6b). Station KLOK is also not affected by small fluctuations observed in the data of borehole S614 (Fig. 6b). There is a clear difference between water levels in west Thessaly (M256, S597 and S614; Fig. 5) and east Thessaly, as the level in the west ranges between − 2 and − 12 m (i.e., much shallower that to the west). We note that our borehole data are limited (both in number of wells and in rates of sampling the level), so more data are necessary to confirm the above results.

It is noticeable that the changes of the ground water level were not caused by a corresponding reduction of the mean rainfalls (Fig. 8). We plot mean monthly rainfall levels (in mm; Fig. 8) from several meteorological stations in Thessaly (four "continental" stations i.e., Klokotos, Trikala, Karditsa and Larissa; one coastal: Volos; see Fig. 1 for locations) that indicate a regular pattern of high–low rainfall without an obvious trend. Meteo stations Karditsa, Trikala and Klokotos recorded systematically higher amounts of rainfall except for the summer of 2017 (Fig. 8). We also note that during the summer of 2015, 2016 and 2017 the mean rainfall exceeded the amount of 100 mm in several meteorological stations (Fig. 8) which is mostly supplied by summer storms, an effect

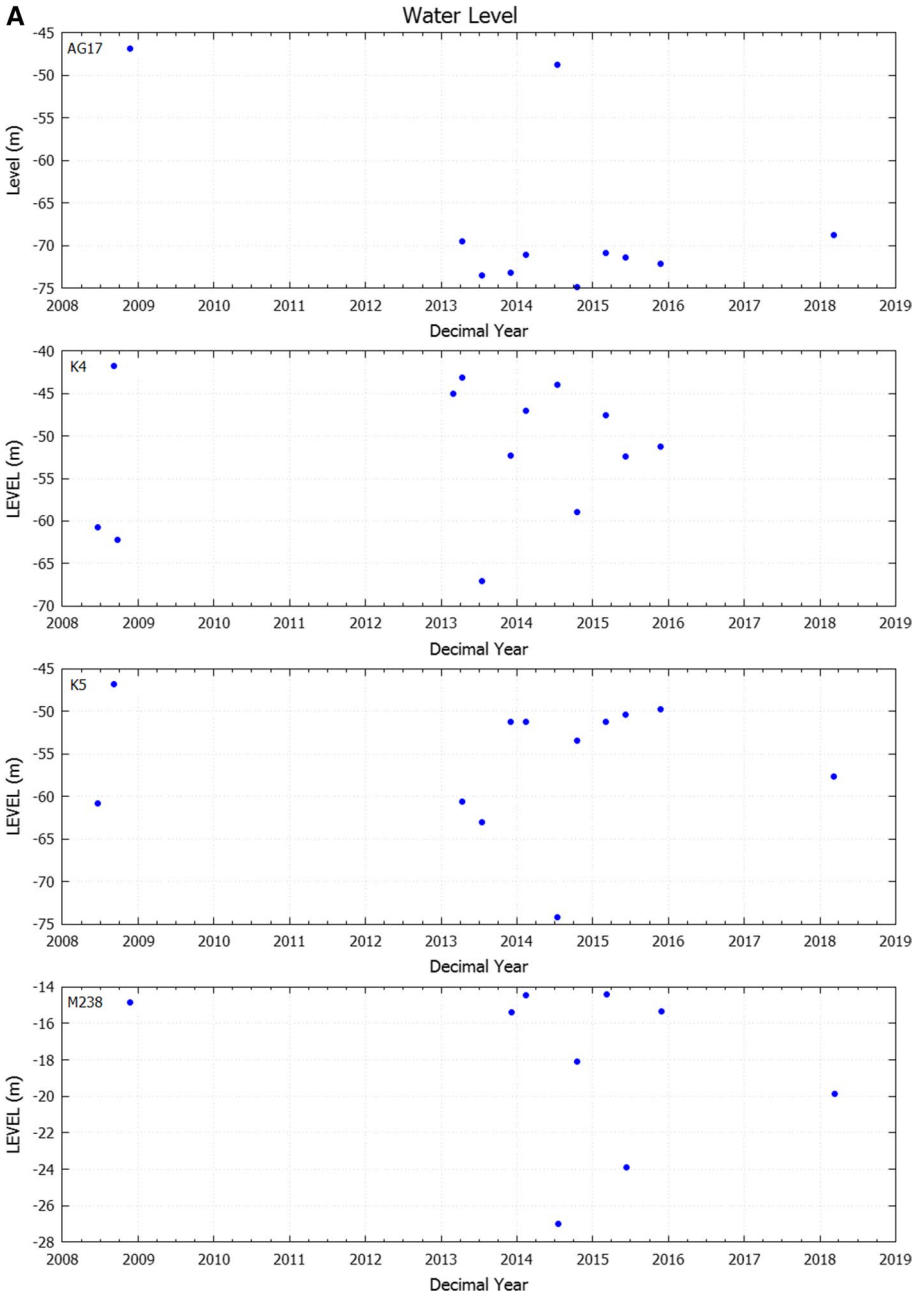

Fig. 6 **a** Graphs showing groundwater variation with time. Borehole names are visible on the upper left corner. Borehole locations are shown in Fig. 5. **b** Graphs showing groundwater variation with time. Borehole names are visible on the upper left corner. Borehole locations are shown in Fig. 5

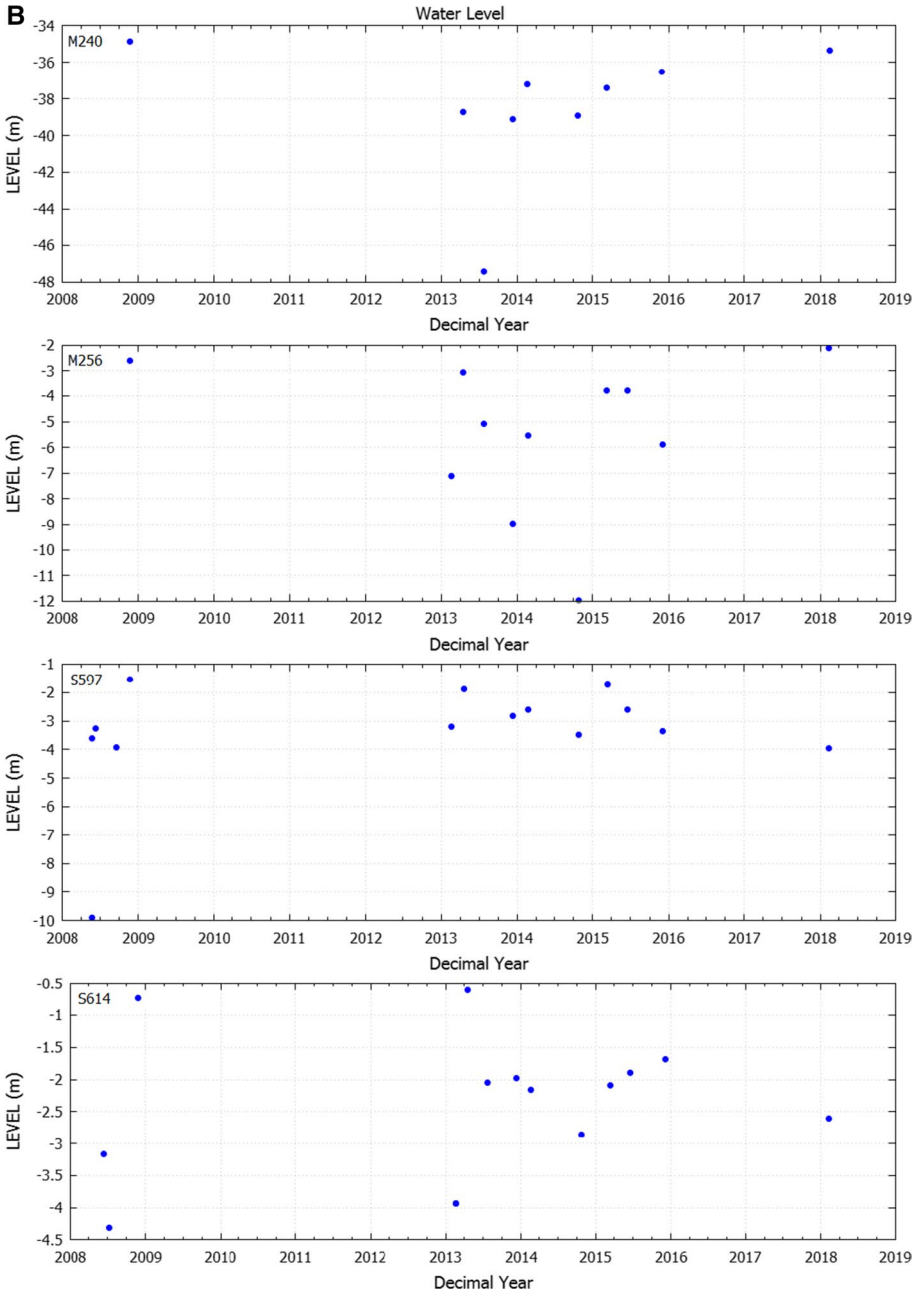

Fig. 6 (continued)

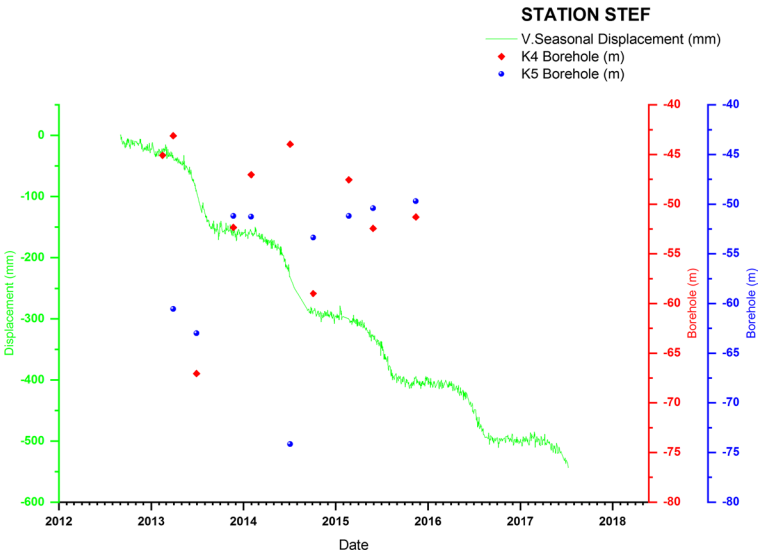

Fig. 7 Graph showing overlay of borehole data K4 (red rhombs) and K5 (blue dots) over the time series of daily vertical position estimates of station STEF. *X*-axis is time (years), *Y*-axis is position (in mm; left) and water levels (in m; right). Notice the drawdown during the summer of 2013, 2014 and 2015 (K4 only) is correlated with the "ramp" part of the height time series. See Fig. 5 for locations

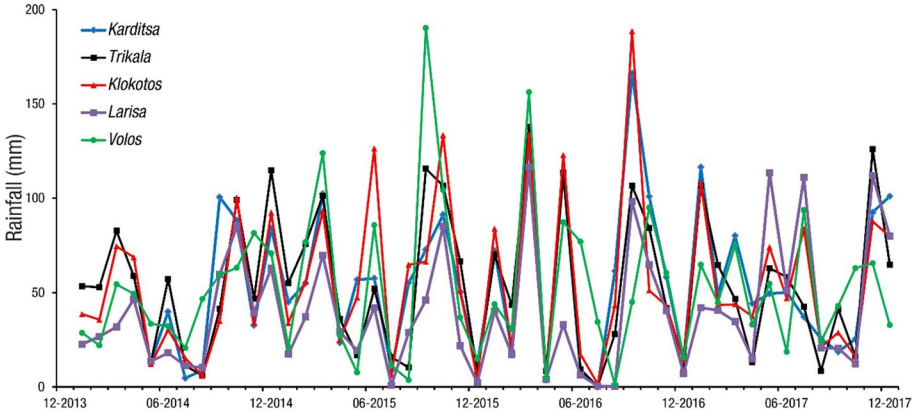

Fig. 8 Graph showing monthly rainfall variation (in mm) with time (period 2014–2017). Meteo station Klokotos is co-located with GNSS station KLOK (Fig. 1). It is observed that all stations follow the same trend with minor exceptions (e.g., station Volos which is a coastal station)

also recognized in older datasets (e.g., Tsimi et al. 2012). The 2013–2018 GNSS data pattern of Thessaly in cross-examination with borehole data of the same period (Fig. 6) could be an indicative of groundwater that is locally depleted because of anthropogenic activities (for example, region of station STEF).

Fig. 9 Correlation graphs for GNSS stations LARM (**a**) KRDI (**b**) and KLOK (**c**) showing variation of three geophysical variables (position, rainfall, groundwater level) with time. Green color scale shows position (in mm), red color scale is rainfall (mm), and blue color scale is groundwater level (in m), respectively ▶

5.2 Correlation of time series

To better understand and analyze the effects of environmental factors (rainfall and groundwater-level variations) we decomposed the vertical time series (position) of three geodetic stations (KLOK, LARM and KRDI) to its components (using R, www.R-project.org/; see supplementary Fig. S4 for station KLOK decomposition). Those stations showed a relative stability in height position with time (Fig. 3). In this way we may discover some subtle correlation among our datasets that is not visually discernible, for example in stations LARM and KRDI. To analyze the vertical position time series we used the STL (seasonal-trend decomposition based on LOESS; Cleveland 1981; Cleveland et al. 1990) procedure (which is part of R software; R Core Team 2014). LOESS is a smoother application sequence whose main advantage is that it allows the processing of very long time series, large amounts of trend and fast computation of seasonal smoothing. In addition, it can handle missing values of time-series decomposition. Also the STL procedure has advantages over other methods because it handles seasonality and can be robust to outliers. After the decomposition we processed the seasonal signal of the time series to find its period; we use sine wave fitting using the formula:

$$y = y0 + A \sin\left(\pi \frac{x - x_c}{w}\right)$$

where y is position, $A > 0$, x_c is phase shift, A is amplitude of the seasonal signal (in mm), w is semi-period (in days), and $y0$ is offset. After several iterations the solution converged and we identified the period of the seasonal signal.

In Fig. 9 we plot the decomposed geodetic data (green dots), the monthly rainfall data (red bars) and the groundwater data (blue dots) for the period 2011–2018. We also fit the seasonal displacement in the geodetic data (black curve), showing that it displays a periodicity for all three stations. Indeed, a good correlation between groundwater level and geodetic displacement is observed for station KRDI (period 2013–2016); except for one data point in the April of 2013 the curve follows the water-level fluctuations. We also see no correlation with rainfall for KRDI (for example see year 2017 where rainfall amount is reduced between January and August, but geodetic height is increased). In all three stations the amplitude of the seasonal signal (the black curve) is ± 5 mm, that is the modeled height (position) variations through time do not exceed the value of 5 mm.

Moreover, station KLOK (Fig. 9) shows a displacement periodicity aligned with the seasonal periodicity, i.e., displacement highs are observed in autumn (i.e., October, November) each year and displacement lows in February–March. This remarkable periodicity is not correlated with rainfall patterns nor groundwater-level fluctuations, so we deduce that it reflects geodynamic processes (motions of the plate). KLOK's position is expected to reflect such motions as the station is founded on bedrock (Fig. 2). Stations KRDI and LARM also display periodicities (Table 3); however, they cannot be correlated with particular weather seasons. We also note that those stations are located on buildings that are founded on syn-rift sediments; therefore, it may be possible that groundwater fluctuations are reflected in their behavior.

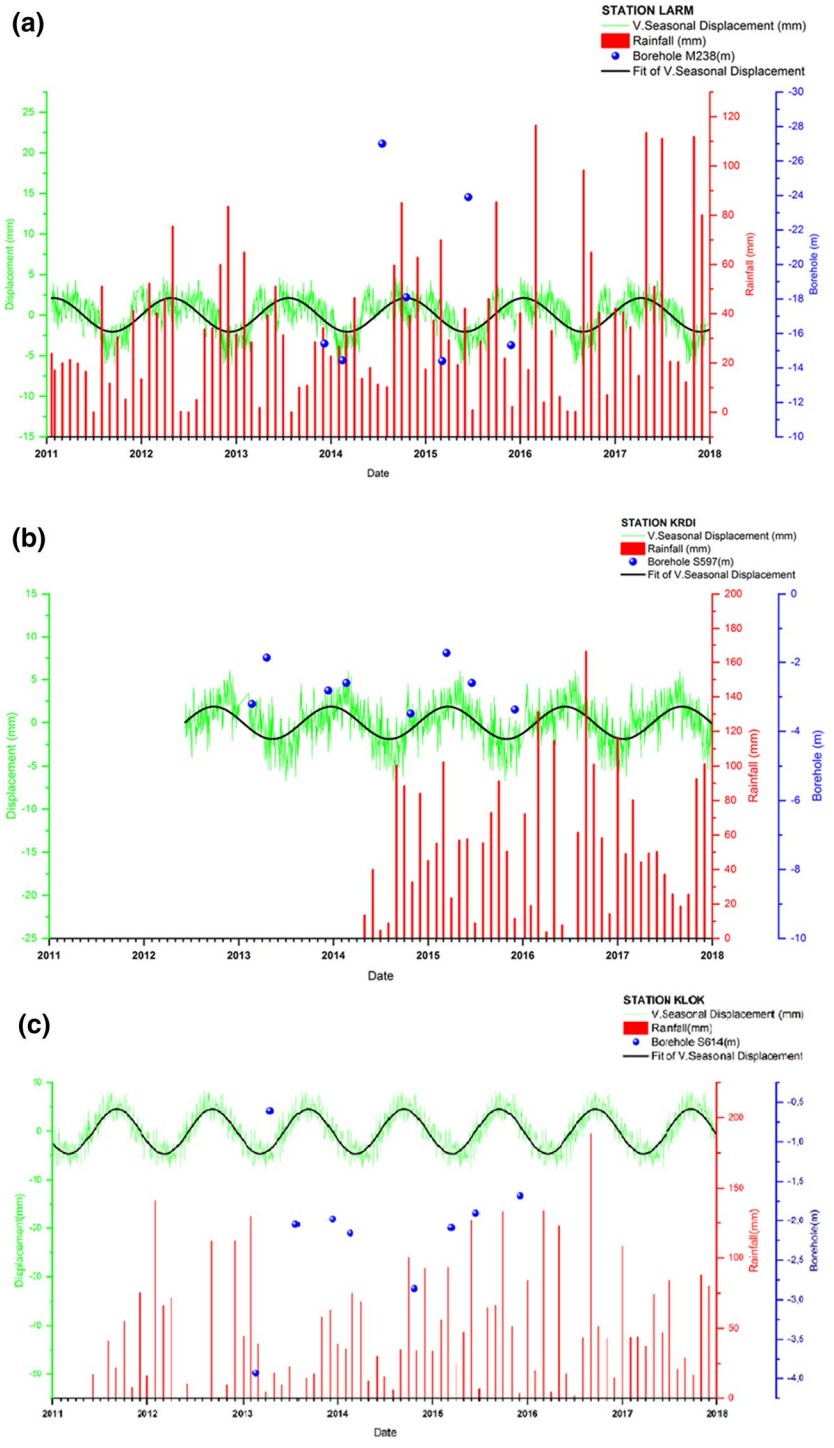
(a)
STATION LARM
V.Seasonal Displacement (mm)
Rainfall (mm)
Borehole M238(m)
Fit of V.Seasonal Displacement
Displacement (mm)
Rainfall (mm)
Borehole (m)
Date
(b)
STATION KRDI
V.Seasonal Displacement (mm)
Rainfall (mm)
Borehole S597(m)
Fit of V.Seasonal Displacement
Displacement (mm)
Rainfall (mm)
Borehole (m)
Date
(c)
STATION KLOK
V.Seasonal Displacement (mm)
Rainfall(mm)
Borehole S614(m)
Fit of V.Seasonal Displacement
Displacement(mm)
Rainfall(mm)
Borehole(m)
Date

Table 3 Estimation of the seasonal parameters of the geodetic data (vertical component of position) of stations KLOK, KRDI and LARM

Station	*y0* (mm)	x_c	*A* (mm)	*w* (days)
KLOK	−0.06496	0	4.574	184.25
KRDI	−0.02777	0	1.881	225.62
LARM	0.03066	0	2.075	226.60

6 Conclusions

1. The most prominent subsidence signal in the Thessaly basin is inside its southeastern part, inside a Quaternary alluvial plain where GNSS station STEF is located (former Karla lake; Figs. 5, 7) which underwent average vertical subsidence at ~ 10 cm/yr during 2012–2017. The cumulative subsidence reached 55 cm in 2017.
2. Surface subsidence at STEF is correlated with groundwater-level drawdown but not with rainfall patterns, i.e., it is anthropogenically induced because of overexploitation of the ground water.
3. Correlation analysis of stations KLOK, KRDI and LARM using seasonal-trend decomposition procedure based on LOESS smoothing showed that KRDI and LARM height pattern reflects groundwater fluctuations.
4. The periodicity observed in geodetic data of station KLOK is not correlated with either groundwater levels or rainfall patterns; therefore, it reflects geodynamic processes.

Acknowledgements The NOANET network was funded by several EU and national research projects from the General Secretariat for Research and Technology of Greece (GSRT). The KLOK station has been set up in Greece by INGV (Marco Anzidei with Athanassios Ganas of NOA) for the extension of the CGPS networks in the Mediterranean region. The geodetic equipment of station STEF is property of the Laboratory of Higher Geodesy, National Technical University of Athens (NTUA). We acknowledge useful comments by Christina Tsimi, Riccardo Caputo, Geoff Blewitt, Marco Anzidei, Efthimios Lekkas, Panagiotis Grigorakakis and Alekos Belesis. We acknowledge support of this research by the project "HELPOS - Hellenic Plate Observing System" (MIS 5002697) which is implemented under the Action "*Reinforcement of the Research and Innovation Infrastructure,*" funded by the Operational Programme "*Competitiveness, Entrepreneurship and Innovation*" (NSRF 2014-2020) and co-financed by Greece and the European Union (European Regional Development Fund). P. Argyrakis acknowledges the Stavros Niarchos Foundation for its support. We thank George Manthos (IGME) for his help with groundwater data. We thank www.meteo.gr for making available their rainfall measurements. We thank Kostas Giannikis for his help with station KLOK maintenance. The geodetic data are available for download from the NOA GSAC facility http://194.177.194.238:8080/noanetgsac/.

References

Ambraseys N, Jackson J (1990) Seismicity and associated strain of central Greece between 1890 and 1988. Geophys J Int 101(3):663–708. https://doi.org/10.1111/j.1365-246X.1990.tb05577.x

Apostolidis E, Koukis G (2013) Engineering-geological conditions of the formations in the Western Thessaly basin, Greece. Central Eur J Geosci 5(3):407–422

Argus DF, Fu Y, Landerer FW (2014) Seasonal variation in total water storage in California inferred from GPS observations of vertical land motion. Geophys Res Lett 41:1971–1980. https://doi.org/10.1002/2014GL059570

Atzori S, Salvi S, Stramondo S, Tolomei C, Hunstad I, Ganas A (2005) Estimation of slow ground movements using the SBAS and PS techniques: examples from Central Italy and Thessaly, Greece. Discussion Meeting Abstracts: The impact of satellite measurements on the observation and modeling of continental deformation. Organised by COMET, 10-11 February 2005, London, UK

Bertiger W, Desai S, Haines B, Harvey N, Moore A, Owen S, Weiss J (2010) Single receiver phase ambiguity resolution with GPS data. J Geodesy 84(5):327–337. https://doi.org/10.1007/s00190-010-0371-9

Caputo R (1990) Geological and structural study of the recent and active brittle deformation of the Neogene-Quaternary basins of Thessaly (Central Greece). In: Scientific Annals, Aristotle University of Thessaloniki, 255 pp., 5 encl., 2 vol., Thessaloniki

Caputo R, Pavlides S (1993) Late Cenozoic geodynamic evolution of Thessaly and surroundings (Central-Northern Greece). Tectonophysics 223(3–4):339–362

Caputo R, Bravard J-P, Helly B (1994) The Pliocene-Quaternary tecto-sedimentary evolution of the Larissa Plain (Eastern Thessaly, Greece). Geodin Acta 7(2):57–85

Caputo R, Helly B, Pavlides S, Papadopoulos G (2004) Seismological investigation of the Tyrnavos Fault (Thessaly, Central Greece). Tectonophysics 394(1–2):1–20

Chen W, Braitenberg C, Serpelloni E (2018) Interference of tectonic signals in subsurface hydrologic monitoring through gravity and GPS due to mountain building. Global Planet Change 167:148–159. https://doi.org/10.1016/j.gloplacha.2018.05.003

Chousianitis K, Ganas A, Gianniou M (2013a) Kinematic interpretation of present-day crustal deformation in central Greece from continuous GPS measurements. J Geodyn 71:1–13

Chousianitis K, Ganas A, Papanikolaou M, Argyrakis P, Drakatos G, Makropoulos K (2013b) Time series analysis of the NOANET CGPS stations. Bull Geol Soc Greece 47(2):508–517. https://doi.org/10.12681/bgsg.11078

Chousianitis K, Ganas A, Evangelidis CP (2015) Strain and rotation rate patterns of mainland Greece from continuous GPS data and comparison between seismic and geodetic moment release. J Geophys Res Solid Earth 120:3909–3931

Clarke PJ et al (1998) Crustal strain in central Greece from repeated measurements in the interval 1989–1997. Geophys J Int 135:195–214

Cleveland W (1981) LOWESS: a program for smoothing scatterplots by robust locally weighted regression. Am Stat 35(1):54. https://doi.org/10.2307/2683591

Cleveland RB, Cleveland WS, McRae JE, Terpenning IJ (1990) STL: a seasonal-trend decomposition procedure based on loess. J Off Stat 6(1):3–33

Devoti R et al (2017) A combined velocity field of the mediterranean region. Ann Geophys 60(2):S0215

Drakos AG, Stiros SC, Kiratzi AA (2001) Fault parameters of the 1980 (M-w 6.5) Volos, central Greece, earthquake from inversion of repeated leveling data. Bull Seismol Soc Am 91(6):1673–1684. https://doi.org/10.1785/0120000232

Estey LH, Meertens CM (1999) TEQC: the multi-purpose toolkit for GPS/GLONASS data. GPS Solut 3(1):42–49. https://doi.org/10.1007/PL00012778

Foumelis M, Papageorgiou E, Stamatopoulos C (2016) Episodic ground deformation signals in Thessaly Plain (Greece) revealed by data mining of SAR interferometry time series. Int J Remote Sens 37(16):3696–3711. https://doi.org/10.1080/01431161.2016.1201233

Ganas A, Drakatos G, Rontogianni S, Tsimi C, Petrou P, Papanikolaou M, Argyrakis P, Boukouras K, Melis N, Stavrakakis G (2008) NOANET: the new permanent GPS network for Geodynamics in Greece. Geophys Res Abstr 10, EGU2008-A-04380

Ganas A, Salvi S, Stramondo S, Lanari R (2004) Monitoring long-term ground deformation in Thessaly (central Greece) by SAR interferometry. In: Abstracts of the DRAGON Project Conference, Athens, 11 October 2004

Ganas A, Salvi S, Atzori S, Tolomei C (2006) Ground deformation in Thessaly, Central Greece, retrieved from Differential Interferometric analysis of ERS-SAR data. In: 11th international symposium on natural and human induced hazards & 2nd workshop on earthquake prediction abstract volume, June 22–25, 2006, Patras, Greece

Ganas A, Oikonomou IA, Tsimi X (2013a) NOAfaults: a digital database for active faults in Greece. Bull Geol Soc Greece 47(2):518–530. https://doi.org/10.12681/bgsg.11079

Ganas A, Marinou A, Anastasiou D, Paradissis D, Papazissi K, Tzavaras P, Drakatos G (2013b) GPS-derived estimates of crustal deformation in the central and north Ionian Sea, Greece: 3-yr results from NOANET continuous network data. J Geodyn 67:62–71. https://doi.org/10.1016/j.jog.2012.05.010

Ganas A, Karastathis V, Moshou A, Valkaniotis S, Mouzakiotis E, Papathanassiou G (2014) Aftershock relocation and frequency-size distribution, stress inversion and seismotectonic setting of the 7 August 2013 M = 5.4 earthquake in Kallidromon Mountain, central Greece. Tectonophysics 617:101–113

Ganas A, Chousianitis K, Argyrakis P, Tsimi C, Papanikolaou M, Papathanassiou G, Exarchos K (2016) Monitoring of surface displacements in the Kalochori area (Thessaloniki, Greece) using a local GNSS network. Bull Geol Soc Greece 50(3):1553–1562. https://doi.org/10.12681/bgsg.11869

Ganas A, Andritsou N, Kosma C, Argyrakis P, Tsironi V, Drakatos G (2018a) A 20-yr database (1997-2017) of co-seismic displacements from GPS recordings in the Aegean area and their scaling with Mw and hypocentral distance. Bull Geol Soc Greece 52:98–130. https://doi.org/10.12681/bgsg.18070

Ganas A, Kourkouli P, Briole P, Moshou A, Elias P, Parcharidis I (2018b) Coseismic displacements from moderate-size earthquakes mapped by Sentinel-1 differential interferometry: the case of February 2017 Gulpinar Earthquake Sequence (Biga Peninsula, Turkey). Remote Sens 10(7):1089

Hatzfeld D, Ziazia M, Kementzetzidou D, Hatzidimitriou P, Panagiotopoulos D, Makropoulos K (1999) Microseismicity and focal mechanisms at the western termination of the North Anatolian Fault and their implications for continental tectonics. Geophys J Int 137(3):891–908

Hill EM, Blewitt G (2006) Testing for fault activity at Yucca Mountain, Nevada, using independent GPS results from the BARGEN network. Geophys Res Lett 33:L14302. https://doi.org/10.1029/2006GL026140

Ilia I, Loupasakis C, Tsangaratos P (2016) Assessing ground subsidence phenomena with persistent scatterer interferometry data in western Thessaly, Greece. Bull Geol Soc Greece 50(3):1693–1702. https://doi.org/10.12681/bgsg.11892

Ilia I, Loupasakis C, Tsangaratos P (2018) Land subsidence phenomena investigated by spatiotemporal analysis of groundwater resources, remote sensing techniques, and random forest method: the case of Western Thessaly, Greece. Environ Monit Assess 190:623. https://doi.org/10.1007/s10661-018-6992-9

Kahle H-G, Cocard M, Peter Y, Geiger A, Reilinger R, Barka A, Veis G (2000) GPS-derived strain rate field within the boundary zones of the Eurasian, African and Arabian Plates. J Geophys Res 105(10):23353–23370

Kaplan E, Hegarty C (2006) Understanding GPS principles and applications, 2nd edn. Artech House Inc, Norwood, p 683

Kontogianni V, Pytharouli S, Stiros S (2007) Ground subsidence, Quaternary faults and vulnerability of utilities and transportation networks in Thessaly, Greece. Environ Geol 52(6):1085–1095. https://doi.org/10.1007/s00254-006-0548-y

Loukas A, Mylopoulos N, Vasiliades L (2007) A modeling system for the evaluation of water resources management strategies in Thessaly, Greece. Water Resour Manage 21:1673. https://doi.org/10.1007/s11269-006-9120-5

Manakos A, Tsioumas V (2010) Hydrogeological study of Thessaly Water Basin (08). Institute of Mineral and Geological Exploration, Thessaloniki. 606 pp (**in Greek**)

Manakos A, Ntona MM, Kazakis N, Chalikakis K (2019) Enhanced characterization of the Krania-Elassona structure and functioning allogenic Karst Aquifer in Central Greece. Geosciences 9:15

Marinou A, Ganas A, Papazissi K, Paradissis D (2015) Strain patterns along the Kaparelli-Asopos rift (central Greece) from campaign GPS data. Ann Geophys 58(2):S0219

McClusky S et al (2000) Global positioning system constraints on plate kinematics and dynamics in the eastern Mediterranean and Caucasus. J Geophys Res 105(B3):5695–5719

Modis K, Sideri D (2015) Spatiotemporal estimation of land subsidence and ground water level decline in West Thessaly basin, Greece. Nat Hazards 76:939. https://doi.org/10.1007/s11069-014-1528-2

Mountrakis D, Killias A, Pavlides S, Zouros N, Spyropoulos N, Tranos M, Soulakellis N (1993) Field study of the Southern Thessaly highly active fault zone. In: Proceedings 2nd congress, Greek Association of Geophysicists, Florina

Nyst M, Thatcher W (2004) New constraints on the active tectonic deformation of the Aegean. J Geophys Res 109:B11406. https://doi.org/10.1029/2003JB002830

Palyvos N, Pavlopoulos K, Froussou E, Kranis H, Pustovoytov K, Forman SL, Minos-Minopoulos D (2010) Paleoseismological investigation of the oblique-normal Ekkara ground rupture zone accompanying the M 6.7–7.0 earthquake on 30 April 1954 in Thessaly, Greece: archaeological and geochronological constraints on ground rupture recurrence. J Geophys Res 115:B06301. https://doi.org/10.1029/2009JB006374

Papastamatiou D, Mouyaris N (1986) The earthquake of April 30, 1954, in Sophades (Central Greece). Geophys J R Astron Soc 87:885–895

Papazachos BC, Panagiotopoulos DG, Tsapanos TM, Mountrakis DM, Dimopoulos GC (1983) A study of the 1980 summer seismic sequence in the Magnesia region of Central Greece. Geophys J Int 75(1):155–168. https://doi.org/10.1111/j.1365-246X.1983.tb01918.x

Papazachos BC, Hatzidimitriou PM, Karakaisis GF, Papazachos CB, Tsokas GN (1993) Rupture zones and active crustal deformation in southern Thessalia, central Greece. Boll Geof Teor Appl 139:363–374

Papazachos G, Papazachos C, Skarlatoudis A et al (2016) Modelling macroseismic observations for historical earthquakes: the cases of the M = 7.0, 1954 Sofades and M = 6.8, 1957 Velestino events (central Greece). J Seismol 20:151. https://doi.org/10.1007/s10950-015-9517-9

Parcharidis I, Foumelis M, Katsafados P (2011) Seasonal ground deformation monitoring over Southern Larissa Plain (Central Greece) by SAR interferometry. In: Lambrakis N, Stournaras G, Katsanou K (eds) Advances in the research of aquatic environment. Environmental Earth Sciences. Springer, Berlin

Pavlides SB (1993) Active faulting in multi-fractured seismogenic areas, examples from Greece. Z Geomorph N F Suppl Bd 94:57–72

Pavlides S, Kouskouna V, Ganas A, Caputo R, Karastathis V, Sokos E (2004) The Gonnoi (NE Thessaly—Greece) Earthquake (June 2003, Ms = 5.5) and the neotectonic regime of lower olympus. In: 5th international symposium on eastern mediterranean geology, Thessaloniki, Greece, pp 627–630

R Core Team (2014) R: A language and environment for statistical computing. R Foundation for Statistical Computing, Vienna, Austria. http://www.R-project.org/

Rapti-Caputo D, Caputo R (2004) Some remarks on the formation of ground fissures in Thessaly, Greece. In: Proceedings of the 5th international symposium on eastern mediterranean geology, Thessaloniki, Greece, pp 1016–1019

Rózsa, S. (2014). Modelling Tropospheric Delays Using the Global Surface Meteorological Parameter Model GPT2. Periodica Polytechnica Civil Engineering, 58(4), 301–308. https://doi.org/10.3311/PPci.7267

Salvi S, Ganas A, Stramondo S, Atzori S, Tolomei C, Pepe A, Manzo M, Casu F, Berardino P, Lanari R (2004) Monitoring long-term ground deformation by SAR interferometry: Examples from the Abruzzi, Central Italy, and Thessaly, Greece. In: 5th international symposium on eastern mediterranean geology, Thessaloniki, Greece, Reference T7-17

Seferli S, Modis K, Adam K (2019) Interpretation of groundwater hydrographs in the West Thessaly basin, Greece, using principal component analysis. Environ Earth Sci 78:257. https://doi.org/10.1007/s12665-019-8262-8

Serpelloni E, Anzidei M, Baldi P et al (2005) Crustal velocity and strain-rate fields in Italy and surrounding regions: new results from the analysis of permanent and non-permanent GPS networks. Geophys J Int 161:861–880. https://doi.org/10.1111/j.1365-246X.2005.02618.x

Serpelloni E, Pintori F, Gualandi A, Scoccimarro E, Cavaliere A, Anderlini L, Belardinelli ME, Todesco M (2018) Hydrologically induced karst deformation: insights from GPS measurements in the Adria-Eurasia Plate Boundary Zone. J Geophys Res Solid Earth 123:5. https://doi.org/10.1002/2017JB015252

Sidiropoulos P, Mylopoulos N, Loukas A (2013) Optimal management of an overexploited aquifer under climate change: the Lake Karla case. Water Resour Manag 27(6):1635–1649. https://doi.org/10.1007/s11269-012-0083-4

Soulios G (1997) Subsidence de terrains alluviaux dans le sud-est de la plaine de Thessalie, Grece. In: Marinos K, Stournaras T (eds) Engineering geology and the environment, Balkema, pp 1067–1072

Stamatopoulos C, Petridis P, Parcharidis I et al (2018) A method predicting pumping-induced ground settlement using back-analysis and its application in the Karla region of Greece. Nat Hazards 92:1733. https://doi.org/10.1007/s11069-018-3276-1

Steigenberger P, Boehm J, Tesmer V (2009) Comparison of GMF/GPT with VMF1/ECMWF and implications for atmospheric loading. J Geodesy. https://doi.org/10.1007/s00190-009-0311-8

Tsimi Ch, Ganas A, Dimoyiannis D, Valmis S, Lekkas E (2012) Catchment-wide estimate of single storm interrill soil erosion using an aggregate instability index: a model based on geographic information systems. Nat Hazards 62(3):863–875

Tsodoulos I, Chatzipetros A, Koukouvelas I, Caputo R, Pavlides S, Stamoulis K, Gallousi C, Papachristodoulou C, Ioannides K, Belesis A, Kremastas E, Kalyvas D (2016) Palaeoseismological investigation of the Gyrtoni fault (Thessaly, central Greece). Bull Geol Soc Greece 50(1):552–562. https://doi.org/10.12681/bgsg.11755

Upton G, Cook I (1996) Understanding statistics. Oxford University Press, Oxford, p 55

Ustun A, Tusat E, Yalvac S (2010) Preliminary results of land subsidence monitoring project in Konya Closed Basin between 2006–2009 by means of GNSS observations. Nat Hazards Earth Syst Sci 10(6):1151–1157. https://doi.org/10.5194/nhess-10-1151-2010

Vassilopoulou S, Sakkas V, Wegmuller U, Capes R (2013) Long term and seasonal ground deformation monitoring of Larissa Plain (Central Greece) by persistent scattering interferometry. Cent Eur J Geol 5:61. https://doi.org/10.2478/s13533-012-0115-x

Wahr JM (1985) Deformation induced by polar motion. J Geophys Res 90(B11):9363–9368. https://doi.org/10.1029/JB090iB11p09363

Wang M, Li B (2016) Evaluation of empirical tropospheric models using satellite-tracking tropospheric wet delays with water vapor radiometer at Tongji, China. Sensors (Basel) 16(2):186. https://doi.org/10.3390/s16020186

Williams SDP (2008) CATS, GPS coordinate time series analysis software. GPS Solut 12:147–153. https://doi.org/10.1007/s10291-007-0086-4

Wu D, Yan H, Shen Y (2017) TSAnalyzer, a GNSS time series analysis software. GPS Solut 21:1389–1394. https://doi.org/10.1007/s10291-017-0637-2

Zerbini S, Richter B, Rocca F, van Dam T, Matonti F (2007) A combination of space and terrestrial geodetic techniques to monitor land subsidence: case study, the Southeastern Po Plain, Italy. J Geophys Res 112:B05401. https://doi.org/10.1029/2006JB004338

Zouros N, Pavlides S, Chatzipetros A (1994) Recent movement on the Larissa plain neotectonic faults (Thessaly, C. Greece). Water-level fluctuation or tectonic creep. XXIV Gen. As. European Seismological Com. Abstracts p. 67

Zumberge JF, Heflin MB, Jefferson DC, Watkins MM, Webb FH (1997) Precise point positioning for the efficient and robust analysis of GPS data from large networks. J Geophys Res 102(B3):5005–5017. https://doi.org/10.1029/96JB03860

Affiliations

Panagiotis Argyrakis[1,2] · Athanassios Ganas[2] · Sotirios Valkaniotis[3] · Vasilios Tsioumas[4] · Nikolaos Sagias[1] · Basil Psiloglou[5]

Athanassios Ganas
aganas@noa.gr

Vasilios Tsioumas
tsioumas@igme.gr

Nikolaos Sagias
nsagias@uop.gr

Basil Psiloglou
bill@noa.gr

[1] Department of Informatics and Telecommunications, University of Peloponnese, Tripoli, Greece

[2] Institute of Geodynamics, National Observatory of Athens, 11810 Athens, Greece

[3] Trikala, Greece

[4] Hydrogeology Section, Institute of Geology and Mineral Exploration, 13677 Athens, Greece

[5] Institute for Environmental Research and Sustainable Development, National Observatory of Athens, I. Metaxa & Vas. Pavlou, 15236 Palea Penteli, Greece